WSRC-MS-2004-00172

Comparison of Residual Saturation and Capillary Pressure Model with UNSODA Data

James E. Laurinat

Savannah River Technology Center
Westinghouse Savannah River Company
Aiken, South Carolina 29808
Phone: 803-725-8052
Fax: 803-725-2756
E-mail address: james.laurinat@srs.gov
February 20, 2004

Westinghouse Savannah River Company
Savannah River Site
Aiken, South Carolina 29808

Comparison of Residual Saturation and Capillary Pressure Model with UNSODA Data

Abstract

Data from the UNSODA unsaturated soil database are compared with predictions from a previously derived capillary pressure model. The model expresses the capillary pressure as a function of a characteristic pore pressure and the wetting phase saturation. The model defines residual wetting and nonwetting saturations and includes separate pressures for imbibition and drainage to account for capillary hysteresis. The pressure gradient for the wetting phase defines the imbibition pressure, and the nonwetting phase pressure gradient defines the drainage pressure.

The capillary pressure model correlates drainage and imbibition data from the UNSODA database, provided that the data incorporate the entry head, a minimum displacement required for drainage to begin. According to the model, the imbibition pressure equals the drainage pressures at a critical minimum saturation of 0.301; below this critical saturation, no additional reversible drainage should occur. Some of the UNSODA data sets had a minimum saturation approximately half this value. The difference is attributed to the presence of fissures, which would lower the residual wetting and critical minimum saturations by reducing the fraction of the void volume controlled by capillary pores. If the UNSODA saturations are adjusted for this discrepancy, a probability distribution of minimum saturations for each data set peaks near the predicted critical minimum

saturation. Maximum saturations for each data set have a peak near the predicted residual nonwetting saturation of 0.884.

The capillary pressure model utilizes a single fitting parameter, a characteristic pore pressure, which can be related to a characteristic pore diameter by Darcy's law. Regression of the UNSODA data shows that this pore diameter approximately equals the mean particle diameter.

Key words:
capillary pressure
residual saturation
hysteresis
model
database

Introduction

Previously, the author developed a model that uses a characteristic pore pressure to predict residual wetting and nonwetting saturations and capillary imbibition and drainage pressures (Laurinat, 2004). The model is based on an energy balance that equates changes in potential surface energy to changes in pressure-volume work. In the model, a simple probabilistic distribution expresses capillary forces as a function of the relative saturation and the characteristic pore pressure. Pressure gradients are derived from

Darcy's law. Limiting imbibition pressures are based on flow of the wetting, or liquid, phase, and limiting drainage pressures are based on flow of the nonwetting, or gas, phase. The model implicitly assumes that the soil is homogeneous and isotropic.

The model predicts a residual wetting saturation, s_{rw}, of 0.236 and a residual nonwetting saturation, s_{rn}, of 0.884. The derived expressions for the limiting capillary pressures for imbibition, $P_{c,i}$, and drainage, $P_{c,d}$, are:

$$\frac{P_{c,i}}{P_c} = \frac{P_{c,i,0}}{P_c} - \frac{ln(s)}{s} \tag{1}$$

and

$$\frac{P_{c,d}}{P_c} = \frac{P_{c,i,0}}{P_c} + \frac{1}{s_{rn}} - \frac{ln(s_{rn})}{s_{rn}} + \frac{(1-s)[1+ln(1-s)] - s\,ln(s)}{s} - \frac{(1-s_{rn})[1+ln(1-s_{rn})] - s_{rn}\,ln(s_{rn})}{s_{rn}} \tag{2}$$

where P_c is the characteristic pore pressure and $P_{c,i,0}$ is the entry head required to initiate imbibition into the soil. It is argued that the entry head equals the vector sum of the characteristic pore pressure acting in all three directions at the soil surface. According to this argument,

$$\frac{P_{c,i,0}}{P_c} = \sqrt{3} \tag{3}$$

The model defined in the preceding equations accurately correlates limiting imbibition and drainage pressures in a selected laboratory test that used a uniformly packed, sieved sand (Smiles et al., 1971; Vachaud and Thony, 1971). In particular, the model predicts that there is a critical saturation, s_{cr}, of 0.301, below which the imbibition pressure exceeds the drainage pressure. Logic dictates that a soil will not drain to any lower saturation, provided that soil remains in contact with liquid. Indeed, measured saturations for the cited imbibition and drainage tests did not fall below this critical saturation.

To apply the model derived for the Smiles et al. data, it is necessary to show that it is valid for other capillary measurements as well. The UNSODA database (Nemes et al., 1999, 2001) maintained by the George E. Brown, Jr., Salinity Laboratory of the U. S. Department of Agriculture, was selected for comparison with the model. The UNSODA database includes both laboratory and field capillary pressure data, conveniently grouped into measurements performed during imbibition and drainage. The database contains 137 field drainage data sets, 2 field imbibition data sets, 730 laboratory drainage data sets, and 33 laboratory imbibition data sets. Soils represented in the UNSODA database range from uniform, single-grain size sands used for laboratory tests to sand, loam, and clay soils and mixtures thereof. The database lists pressure measurements in inches water as functions of the bulk water saturation θ, defined as the liquid volume divided by the total volume of the porous material.

A limited number of data sets in the UNSODA database report the bulk and theoretical solid density for the porous material. For these data sets the total porosity, θ_{max}, can be calculated from these two density measurements, using

$$\theta_{dens} = \frac{\rho_{meas}}{\rho_{th}} \tag{4}$$

The majority of the data sets do not give density measurements, however, so the total porosity for the UNSODA data is not generally known. Consequently, use of these data to evaluate the capillary pressure model requires an assumption about either the minimum or the maximum measured water saturation. For many of the data sets, capillary pressures approach a singularity near the minimum measured water saturation, with the magnitude of the capillary pressure limited only by the atmospheric pressure. Therefore, the minimum saturation should not be used to normalize capillary pressures with respect to the intrinsic pore pressure P_c and is a poor choice on which to base the comparison with the capillary pressure model. By default, then, the maximum measured saturation serves as the basis for comparing the model with the data. The comparisons assume that the maximum measured liquid saturation equals the residual nonwetting saturation. This assumption gives the following formula for converting measured bulk saturations to relative saturations:

$$s = s_{rn} \frac{\theta}{\theta_{max}} \tag{5}$$

where θ_{max} represents the maximum measured saturation for each data set as a fraction of the total bulk volume.

All data from the UNSODA database initially were fit to the capillary pressure model using the reduced saturation given by Equation 5. Not all data sets in the database contain measurements that extend to liquid saturation, so this conversion is not universally valid. However, the fraction of data sets that contain saturated liquid measurements is sufficient for a meaningful comparison.

Comparison of Model with Paired Imbibition and Drainage Measurements from the UNSODA Database

The first data that were fitted were paired imbibition and drainage that exhibited a significant entry head $P_{c,i,0}$. There were five such data sets from four different sources (Shen and Jaynes,1988; Stauffer and Dracos, 1986; Liakopoulos, 1966; Poulovassilis, 1970). All of these data sets contained measurements made in granular material, or sand, as was true for the Smiles et al. (1971) data. The fitting procedure entailed a calculation of the capillary pore pressure P_c, given as the sum of the measured capillary pressures divided by the sum of the capillary pressures predicted by the model at the relative saturations for each measurement. To eliminate measurements near saturation with either liquid or gas, the calculation was limited to relative liquid saturations between 0.4 and 0.75.

Figure 1 compares these data with model predictions. As this figure shows, three data sets (from Shen and Jaynes, Stauffer and Dracos, and Liakopoulos) have minimum measured saturations about half the predicted critical minimum saturation s_{cr}, while the other two data sets (from Poulovassilis) have minimum measured saturations approximately equal to s_{cr}.

The model fits the data closely for the latter two data sets. The most logical explanation for the apparent discrepancy between the minimum measured saturations for the other three data sets and the model prediction is that the porous material develops fissures that fill with gas during drainage. According to this interpretation, the fissures are larger than the pores by a sufficient magnitude that they do not offer any flow resistance but rather simply conduct fluid among the pores. The minimum saturation for a fissured material can be derived by applying a jump condition for the development of fissures. Following the logic used in the analysis of residual wetting saturations, the pressure applied to the liquid phase across such a jump, ΔP_{jump}, is

$$\Delta P_{jump} = P_c\left[\left(1 - s_{min}\right) - \left(1 - s_{cr}\right)\right] = P_c\left(s_{cr} - s_{min}\right) \tag{6}$$

where s_{min} is the minimum liquid saturation for the fissured soil.

The minimum saturation is the saturation that will minimize the free energy associated with this jump, ΔG_{jump}. This free energy, evaluated after the appearance of the fissures, is

$$\Delta G_{jump} = -R_g T \ln\left(P_c s_{min}\left(s_{cr} - s_{min}\right)\right) \tag{7}$$

The value of the critical saturation is fixed by the relative magnitudes of the capillary pressures for imbibition and drainage. Hence, the free energy is minimized when

$$\frac{d\Delta G_{jump}}{ds_{min}} = 0 \tag{8}$$

This condition is satisfied by

$$s_{min} = 0.5 s_{cr} \tag{9}$$

A similar analysis, combined with the observation that the maximum saturation for a homogeneous porous material is the residual nonwetting saturation, gives for the maximum saturation for a fissured soil s_{max},

$$s_{max} = 0.5 + 0.5 s_{rn} \tag{10}$$

The capillary pressure model describes the saturation for just the pores of a fissured material. Because the fissure volume merely conducts pressure among the pores, the overall saturation for the total volume of porous material is a linear function of the pore saturation. If the maximum saturation is defined to be equal to the residual nonwetting saturation to conform with the model, then a linear interpolation between this saturation and the minimum saturation yields the following expression for the overall saturation of a fissured material, s^*, as a function of the model saturation for a homogeneous porous material, s, the residual nonwetting saturation, s_{rn}, and the critical saturation, s_{cr}:

$$s^* = \frac{0.5 s_{cr} s_{rn} - s_{cr} s + s_{rn} s}{s_{rn} - 0.5 s_{cr}} \tag{11}$$

Figure 2 compares the capillary pressure model with the three data sets in outline symbols defined by s^*. The model fits the adjusted imbibition data closely, but two sets of drainage data deviate significantly from the model. The capillary pressures for both of these data sets overshoot the predicted maximum pressure at the critical minimum saturation. The difference between measured and predicted pressures persists even at higher saturations. The discrepancy between the Liakopoulos data and the model gradually diminishes as the saturation increases, so that the data and the model are in approximate agreement at the residual nonwetting saturation. For the Stauffer and Dracos data, on the other hand, the difference between the measured and predicted drainage pressures remains approximately constant as the saturation increases. This suggests the presence of a metastable equilibrium that originates from the upstream (dry) side of the capillary pressure gradient.

The most plausible explanation for the overshoot and apparent metastability phenomena is that at the minimum liquid saturation, the interstitial gas in the fissures begins to exert pressure on the residual liquid in the pores. As explained in the capillary pressure model derivation, this pressure would be the product of the capillary pore pressure P_c and the fraction of the volume occupied by the interstitial gas, $0.5(1-0.5s_{cr})$, divided by the residual pore saturation, $0.5s_{cr}$. Thus, the overshoot pressure $\Delta P_{c,ov}$ is given by

$$\frac{\Delta P_{c,ov}}{P_c} = \frac{1-0.5s_{cr}}{s_{cr}} \tag{12}$$

This overshoot pressure represents the maximum reversible pressure for which both imbibition and drainage can occur. Higher pressures can occur, but only with the application of external suction to the porous material.

The apparent metastability, according to this interpretation, results when the overshoot in the capillary pressure at minimum saturation propagates downstream in the nonwetting (gas) phase. The fraction of the overshoot pressure that propagates would be equal to the fraction of the pore volume occupied by gas, $1-s_{cr}$. If this overshoot pressure propagates, then the metastable drainage pressure $P_{c,d,ms}$ would be given by

$$\frac{P_{c,d,ms}}{P_c} = \frac{P_{c,d}}{P_c} + \frac{(1-s_{cr})(1-0.5s_{cr})}{s_{cr}} \tag{13}$$

Figure 2 shows the predicted overshoot at the minimum saturation and the predicted drainage pressure with the overshoot metastability. The predicted overshoot pressure approximately equals maximum measured pressures, and the Stauffer and Dracos data closely follow the predicted metastable drainage pressure curve.

Data Fitting Procedure for Applying the Capillary Pressure Model to the UNSODA Database

Unlike the paired imbibition and drainage data shown in Figures 1 and 2, most of the remaining data in the UNSODA database do not incorporate the entry head. Apparently, this situation occurs because for many of \these remaining data sets the capillary pressures were measured with reference to the pressure at the highest liquid saturation rather than the gauge pressure for free liquid. To accommodate the absence of the entry head from a portion of the UNSODA data sets, the comparison with the capillary pressure model needs to be at least partially based on changes in the capillary pressure with saturation rather than the total magnitude of the capillary pressure at different saturations.

Accordingly, for each of the remaining data sets, a two-step data fitting procedure was adopted to compare the model with the UNSODA data. The first step consisted of a subtraction of the measured capillary pressure for the relative saturation closest to 0.8, followed by a fit of the resulting reduced pressures. As before, the fitting parameter is

P_c, calculated as the sum of the reduced measured capillary pressures divided by the sum of the capillary pressures predicted by the model at the relative saturations for each measurement. Saturations were calculated using Equation 8. Data sets for which the calculated minimum saturation was less than 0.75 times the critical minimum saturation s_{cr} were modeled as fissured material with adjusted saturations $s*$ given by Equation 11.

To eliminate measurements near either liquid or gas saturation, the calculation was limited to relative liquid saturations between 0.4 and 0.75. Ten iterations were performed to eliminate outliers from the fitting procedure. After the first iteration, normalized capillary pressures less than zero or greater than ten were discarded, as well as any normalized data that differed from predicted pressures by more than 0.5.

The second step began with the total measured capillary pressures, divided by the capillary pore pressure calculated in the first step. For both drainage and imbibition data sets, data were fit to the model with the entry head equal to the predicted value and with the entry head equal to zero. This approach inherently assumes that the database measurements either incorporate the correct entry head or do not account for entry pressure. In other words, the assumption is that the magnitude of the entry head is a question of the reference pressure that is chosen rather than the accuracy of the absolute pressure measurements.

As in the first step, multiplying factors for the second step were calculated by dividing the sum of the reduced pressure measurements by the sum of the capillary pressures predicted by the model. Again, calculations were limited to relative liquid saturations between 0.4 and 0.75, and adjusted pressure measurements less that zero or greater than ten were discarded. These calculations gave two multiplying factors, one for zero entry head and another for the predicted entry head. The multiplying factor with the smaller logarithm was used, and the resulting normalized pressure measurements were compared with the model predictions with or without the entry head, whichever was appropriate. The first and second steps then were repeated to perform additional data filtering.

The two-step screening procedure just described assumes that each data set includes at least one measurement at the residual nonwetting saturation. If this were not true, then the actual saturation would be lower than the calculated saturation, and the pressure increases that occur near the critical minimum saturation would take place at higher saturations, according to the model.

In an effort to eliminate data with maximum measured saturations less than the residual nonwetting saturation, data from each group (field drainage, laboratory drainage, and laboratory imbibition, each both with and without the entry head) were statistically filtered. The filtering consisted of the successive remove of any data sets with data that differed by more than four standard deviations from the model predictions for each group. (Four standard deviations is equivalent to a probability of about 1 in 10,000 for a

normal distribution.) Filtering continued until the number of data sets removed during each pass approached or fell below the expected frequency of 1 in 10,000.

Comparison of Predicted and Measured Imbibition and Drainage Pressures

Figures 3, 4, and 5 compare model predictions with the screened and filtered field drainage, laboratory drainage, and laboratory imbibition data, respectively. The figures portray data from 26 of 137 field drainage data sets, 37 of 730 laboratory drainage data sets, and 21 of 33 laboratory imbibition data sets. Not shown are the results from two field imbibition studies, which covered limited saturation ranges.

Comparisons for field and laboratory drainage data are restricted to those data sets that are better fit using the entry head predicted by the model, while the comparisons for the laboratory imbibition data include both model entry head and zero entry head data fits.

The drainage data comparisons exclude the zero entry head data fits because the pressure multipliers are approximately an order of magnitude smaller than for the data fits that included the entry head and therefore are assumed to be incorrect. The interpretation is that the measured pressures at high saturations did not instantaneously rise to the predicted entry head but instead only gradually approached equilibrium as the saturation decreased. This would result in greater than predicted pressure changes over the range of saturations used for correlation $(0.4 < s < 0.75)$ and a smaller calculated value for the pressure multiplier. Nonequilibrium drainage pressures probably stem from the failure of

the motive fluid, the gas, to wet and maintain contact during the drainage tests. The situation for imbibition differs from that for drainage. During imbibition, the liquid pressure in the porous material quickly equilibrates with the pressure of the surrounding liquid. As a result, the measured pressure always includes the entry head. Reported pressures may or may not incorporate the entry head, depending on whether the reference pressure is taken to be the actual surrounding liquid pressure or the equilibrium pressure at maximum saturation.

A cursory examination of Figures 3, 4, and 5 shows that the capillary pressure model provides reasonable correlations for both imbibition and drainage data over the correlation range $(0.4 < s < 0.75)$. The model also fairly accurately estimates the critical minimum saturation.

Table 1 lists the standard deviations for the differences between model predictions and the screened and filtered data. All data groups have standard deviations between $0.16P_c$ and $0.32P_c$. The largest standard deviation is for the field drainage data including the entry head. The standard deviation for these data is larger because the model underestimates the rate of increase in the drainage pressure as the saturation decreases. Another interpretation of this discrepancy is that the entry head for the field drainage measurements is smaller than predicted by the model. That all of the screened data groupings (except field drainage with the entry head) have approximately the same standard deviation of slightly under $0.2P_c$ suggests that this standard deviation represents

a scatter intrinsic to the data. It also suggests that the model adequately correlates the variation of the capillary pressure with saturation.

Comparison of Predicted and Measured Residual Saturations

These standard deviations provide a valid comparison between measured and predicted capillary pressures at intermediate saturations but are not useful for evaluating the model near the residual nonwetting saturation and the critical minimum saturation, due to large variations in the predicted pressures at these saturations. To assess the predictions of maximum and minimum saturations, probability density functions of the minimum and maximum saturations for each data set were calculated. The density functions are defined as the number of measured minimum or maximum saturation data over a given saturation interval, divided by the total number of measured minimum or maximum saturation data and the interval size.

As explained previously, minimum saturations are calculated based on the assumption that the maximum measured saturation equals the residual nonwetting saturation. This assumption makes it possible to compare minimum saturations for all data sets, whether or not they include measurements of the total porosity. A valid comparison between predicted and measured maximum saturations, on the other hand, requires a measured porosity, obtained from separate measurements of the bulk density and the theoretical solid density. For those data sets modeled as nonfissured soils, i.e., for those data sets

with calculated minimum saturations greater than 0.75 times the critical minimum saturation s_{cr}, the following equation,

$$s = s_{rn} \frac{\theta_{max}}{\theta_{dens}} \tag{14}$$

was used to calculate a "measured" maximum saturation s, with θ_{max} as the porosity equivalent to the maximum measured saturation, and θ_{dens} as the porosity evaluated from density measurements.

For data sets modeled as fissured materials, Equations 37 and 42 combine to yield the following expression for the "measured" maximum saturation:

$$s = \frac{s_{rn}^2}{0.5(1 + s_{rn})} \frac{\theta_{max}}{\theta_{dens}} \tag{15}$$

Figure 6 displays the probability density for the maximum saturations for all the data sets that pass the screening tests and list bulk and solid density measurements. These data sets number about 20 per cent of the total number of UNSODA data sets, 30 of 137 for field drainage tests, 6 of 33 for laboratory imbibition tests, and 186 of 730 for laboratory drainage tests. Three peak frequencies appear in Figure 6. The first peak, at a saturation of 0.885, agrees with the predicted residual nonwetting saturation of 0.884 within the discretization uncertainty of ±0.01. It can be argued that the peaks at higher saturations

represent density measurements for which the porous material was not thoroughly dried, so that the solid volume also included residual liquid in the pores. If this were the case, then the calculated porosity would be less than the actual porosity for dry material, and the calculated maximum saturation would exceed the true maximum saturation.

To account for possible inclusion of residual liquid in the density measurements, all calculated maximum saturations closer to a saturation of one than to the predicted maximum saturation were arbitrarily dropped from consideration. Figure 7 shows a truncated probability density with these measurements eliminated. The truncated distribution includes all of the field drainage tests and laboratory imbibition tests and 114 of the 186 laboratory drainage tests shown in Figure 6. The first peak remains at a saturation of 0.885, with the primary contribution coming from laboratory drainage tests. Saturations for field drainage and laboratory imbibition tests reach their maxima at this saturation.

Figure 8 portrays the probability density for minimum saturations. The minimum saturation frequency peaks at a value of 0.305±0.01, which agrees with the predicted critical minimum saturation of 0.301. A significant tail appears to the right of the peak frequency; and extends to a saturation of about 0.7. This tail probably represents data sets for which measured saturations did not extend down to the critical minimum saturation.

Evaluation of Characteristic Pore Pressures for the UNSODA Data

The final step in development of the capillary pressure model is to relate the characteristic pore pressure P_c derived from the data fit to the particle size of the porous material. (One may recall that, for each data set that was regressed, the pressure multiplier is $\frac{1}{P_c}$.) The UNSODA database includes particle size distributions for a portion of the data sets. Typically, the distributions were measured by sieving, so they are expressed in terms of weight fractions less than a given particle diameter. Integration of these size distributions gives average particle diameters that can be used to correlate pore pressures. The following formula was used to integrate the individual maximum diameters $d_{p,i}$ over the distribution represented by the fractional weights f_i:

$$\bar{d}_p = \frac{0.5 * d_{p,1} f_1 + \sum_{i=2,N} 0.5\left(d_{p,i} + d_{p,i-1}\right)\left(f_i - f_{i-1}\right)}{f_N} \qquad (16)$$

The correlations of pore pressures with these average particle diameters exhibit considerable scatter. Pore pressures correlate better with particle diameters when they are calculated with the inclusion of the entry head than when they are calculated without the entry head. For this reason, efforts to correlate pore pressures were limited to those data sets evaluated with the entry head included.

Figure 9 presents the correlation of pore pressure with particle diameter. Every data set that includes particle diameter data and for which the pore pressure was analyzed with the entry head appears in this figure. All 26 of the field drainage data sets analyzed with the entry head had diameter data. Of 37 such laboratory drainage data sets, 32 had diameter data, and of 21 such laboratory imbibition data sets, 12 had diameters reported. The initial attempt to correlate the pore pressures revealed the presence of several data outliers. A probability rank test identified 16 outliers, including two field drainage pressures, nine laboratory drainage pressures, and five laboratory imbibition pressures.

As Figure 9 shows, a power law function correlates the remaining pore pressures with the diameter raised to the -1.04 power, albeit with a relatively low correlation coefficient of 0.82. According to this power law correlation, then, the pore pressure is approximately inversely proportional to the average particle diameter. This inverse proportionality is consistent with the form of the Laplace relation,

$$P_c = B\frac{4\sigma}{\bar{d}_p} \tag{17}$$

where B is a proportionality constant relating the effective diameter of the voids in the porous material to the average particle diameter. For a simple granular material with most of the voids occurring in the spaces between particles rather than within the particles, the effective void diameter should be of the same magnitude as the particle diameter, so the constant B should be close to one. Indeed, the linear fit shown in Figure 9 yields a best estimate value of 0.92 for B in dimensionless units, with 90% confidence

limits of 0.52 and 1.62. In terms of diameters, the fit yields a characteristic pore diameter that is 1.09 times the mean particle diameter, with 90% confidence limits of 0.62 and 1.92 times the mean particle diameter.

All but one of the regressed data in Figure 9 are for soils types described as “sand’’, “loamy sand”, or “sandy loam”, so the pore diameter correlation needs to be restricted to granular materials. Calculated pore pressures for clay soil types, including five of the outliers shown in Figure 9, generally exceeded values that would be predicted by the linear correlation. Presumably, this occurs because the effective pore diameters for clays are for pores within individual particles or particle agglomerations rather than for spaces between particles. Even for granular materials, the simple linear correlation with average particle diameter may not account for all factors that influence the pore pressure, as evidenced by the low correlation coefficient of 0.72.

Conclusions

The capillary pressure model outlined in this report model correlates both drainage and imbibition pressures reported in the UNSODA database, provided that the pressure measurements account for the entry head. The correlation of imbibition pressures is more satisfactory than the correlation of drainage pressures, probably because internal pressures equilibrate more readily with the entry head during imbibition than during drainage.

The model predicts that liquid saturations should range between a residual nonwetting saturation of 0.884 and a critical minimum saturation of 0.301 at which the drainage pressure equals the imbibition pressure. It is conjectured that, for fissured materials, these limiting saturations need to be adjusted to account for the volume of the fissures, which may occupy half of the total pore volume, according to a force balance. Distributions of maximum and minimum saturations for different UNSODA data sets peak near both the predicted maximum and minimum saturations.

A characteristic pore diameter defines the magnitude of the pressure in the model. For sandy soils, a linear fit of regressed data from UNSODA gives a best estimate characteristic pore diameter that is 1.09 times the mean measured particle diameter. Based on limited data, the pore diameter for clay soils appears to be about an order of magnitude smaller than the mean particle diameter.

In view of the preceding discussion, the model derived in this study accurately correlates capillary pressure data for granular porous media as a function of relative saturation. The model requires only one fitting parameter, a characteristic pore diameter, which approximately equals the mean particle diameter.

Nomenclature

B	ratio of average correlated capillary pore pressure to ideal pore pressure based on Darcy's law
$\bar{d}_p$	volume average particle diameter for porous material
$d_{p,i}$	maximum particle diameter for the ith volume fraction of porous material
f_i	ith volume fraction of porous material, for particle size distribution
ΔG_{jump}	Gibbs free energy associated with jump condition between a homogeneous porous material and a porous material with fissures
P_c	intrinsic capillary pore pressure, equal to the gas-liquid pressure difference
$P_{c,d}$	capillary pressure measured for drainage of the wetting phase
$P_{c,d,ms}$	capillary pressure measured for metastable drainage of the wetting phase
$P_{c,i}$	capillary pressure measured for imbibition of the wetting phase
$P_{c,i,0}$	minimum capillary pressure required to imbibe the wetting phase at the residual nonwetting phase saturation
$\Delta P_{c,ov}$	maximum reversible overshoot in the capillary pressure at the minimum saturation
ΔP_{jump}	pressure change associated with jump condition between a homogeneous porous material and a porous material with fissures, applied to the liquid phase
R_g	universal gas law constant
s	relative saturation with the wetting phase
s^*	saturation for a fissured soil, scaled so that it gives a capillary pressure

	equal to that of a nonfissured soil
s_{cr}	critical saturation where the capillary pressure for imbibition equals the capillary pressure for drainage
s_{max}	maximum saturation for a fissured soil
s_{min}	minimum saturation for a fissured soil
s_{rn}	residual nonwetting phase saturation
s_{rw}	residual wetting phase saturation
T	absolute temperature
θ	liquid saturation as a fraction of the total volume of soil
θ_{dens}	pore volume as a fraction of the total volume of soil, evaluated from bulk and theoretical solids densities
θ_{max}	pore volume as a fraction of the total volume of soil, evaluated from the maximum measured saturation
ρ_{meas}	measured bulk density of soil
ρ_{th}	theoretical density of solids in soil
σ	air-water interfacial tension

Acknowledgment

Dr. G. P. Flach of the Westinghouse Savannah River Company suggested the database comparisons that appear in this paper and provided useful comments during the preparation of the manuscript.

References

Laurinat, J.E. Model for residual saturation and capillary imbibition and drainage pressures. Submitted for publication in J. Hydrol.

Liakopoulos, A.C., 1966. Theoretical approach to the solution of the infiltration problem. Bull. Int. Assoc. Sci. Hydrol. 11(1), 69-110.

Morel-Seytoux, H.J., Khanji, J., Vachaud, G., 1973. Prediction errors due to uncertainties in the measurement and extrapolation of the diffusivity function. Civil Engineering Report, Colorado State University, Fort Collins, CO 80523, CEP72-73, HJM48.

Morel-Seytoux, H.J., Khanji, J., 1975. Prediction of imbibition in a horizontal column. Soil Sci. Soc. Am. Proc. 39, 613-617.

Nemes, A., Schaap, M.G., Leij, F.J., 1999. The UNSODA unsaturated soil hydraulic database, version 2.0. U. S. Salinity Laboratory, U. S. Department of Agriculture, Agricultural Research Service, Riverside, California.

Nemes, A., Schaap, M.G., Leij, F. J., Wosten, J. H. M., 2001. Description of the unsaturated soil hydraulic database UNSODA version 2.0. J. Hydrol. 251(3-4), 151-162.

Poulovassilis, A., 1970. Hysteresis of pore water in granular porous bodies. Soil Sci. 109(1), 5-12.

Shen, R., Jaynes, D. B., 1988. Effect of soil water hysteresis on simulation, infiltration, and distribution, Shuili Xuebao: J. Hydr. Eng. (China) 10, 11-20.

Smiles, D. E., Vachaud, G., Vauclin, M., 1971. A test of the uniqueness of the soil moisture characteristic during transient, nonhysteric, flow of water in a rigid soil. Soil Sci. Soc. Am. Proc. 35, 534-539.

Stauffer, F., Dracos, T., 1986. Experimental and numerical study of water and solute infiltration in layered porous media. J. Hydrol. 84(1-2), 9-34.

Vachaud, G., Thony, J.-L., 1971. Hysteresis during infiltration and redistribution in a soil column at different initial water contents, Water Resour. Res. 7(1), 111-127.

Vauclin, M., 1971. Effets dynamiques sur la relation succion-tenneur en eau lors d'écoulements en milieu non saturé. Thése de Docteur-Ingénieur, Université Scientifique et Médicale de Grenoble.

Table 1. Statistical Evaluation of Differences between Predicted and Measured Capillary Pressures for the UNSODA Database, for Data Filtered by Removing Measurements Deviating from Predicted Values by > 4σ

Data Description	Total Number of Data Sets	Number of Data Sets Correlated	Number of Data Points Correlated	Standard Deviation (σ, P_c)
Field Drainage With Entry Heat	137	26	359	0.32
Laboratory Drainage With Entry Head	730	37	192	0.19
Laboratory Imbibition	33	21	188	
With Entry Head		6	31	0.16
Without Entry Head		15	157	0.17

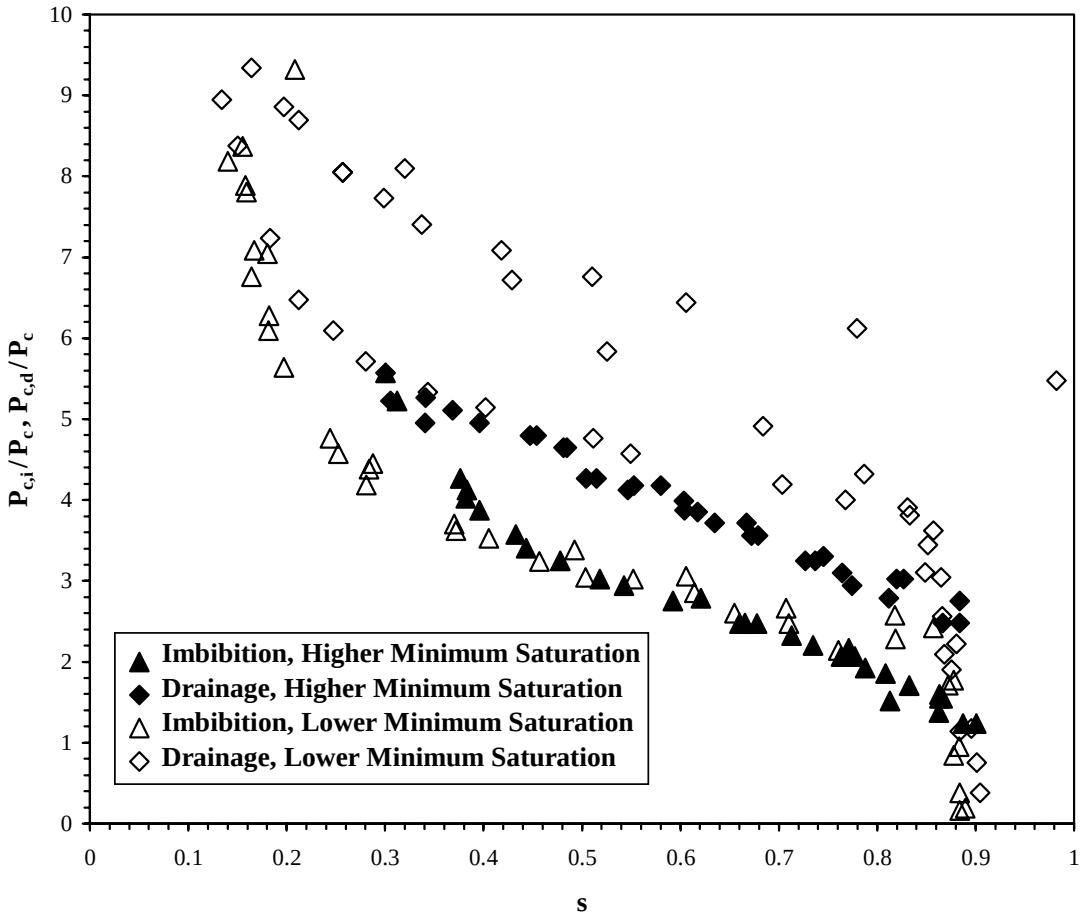

Figure 1. Comparison of UNSODA Paired Imbibition and Drainage

Pressure Data with Predicted Pressures, No Correction for Interstitial Networks

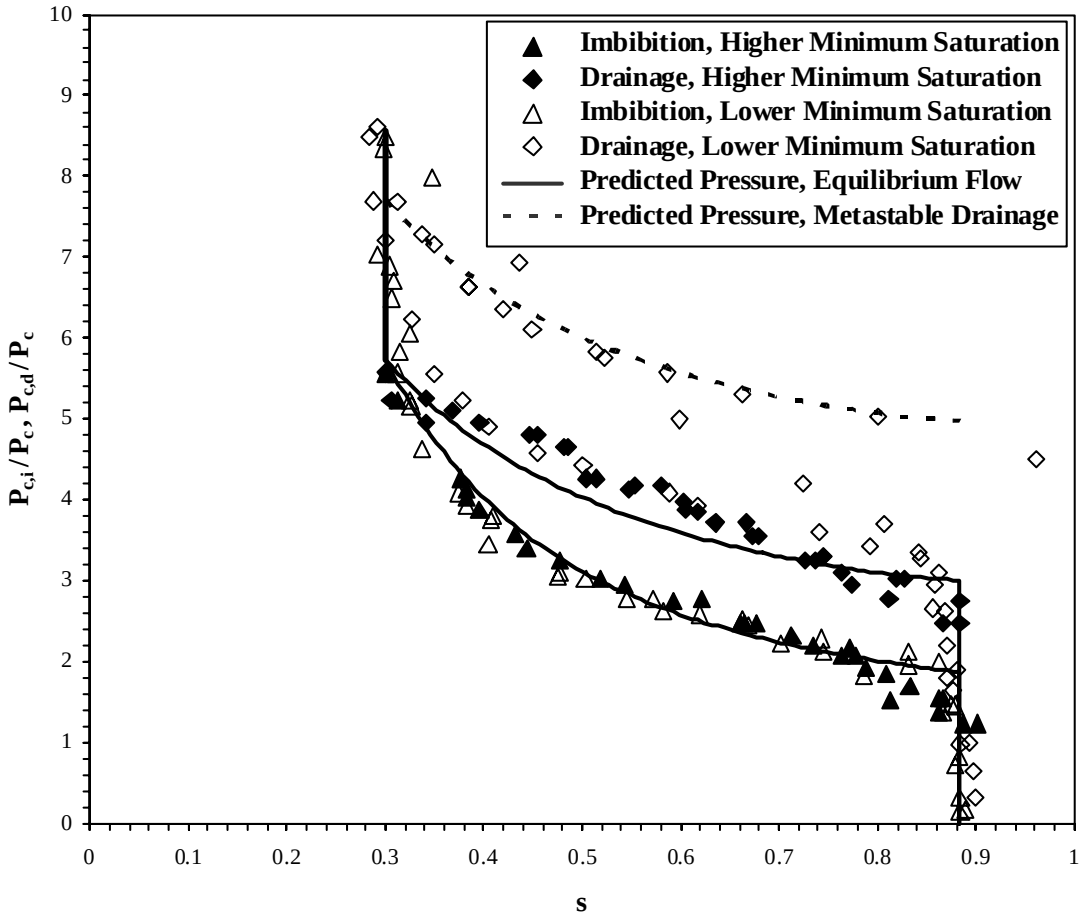

Figure 2. Comparison of UNSODA Paired Imbibition and Drainage Pressure Data with Predicted Pressures, Including Correction for Interstitial Networks

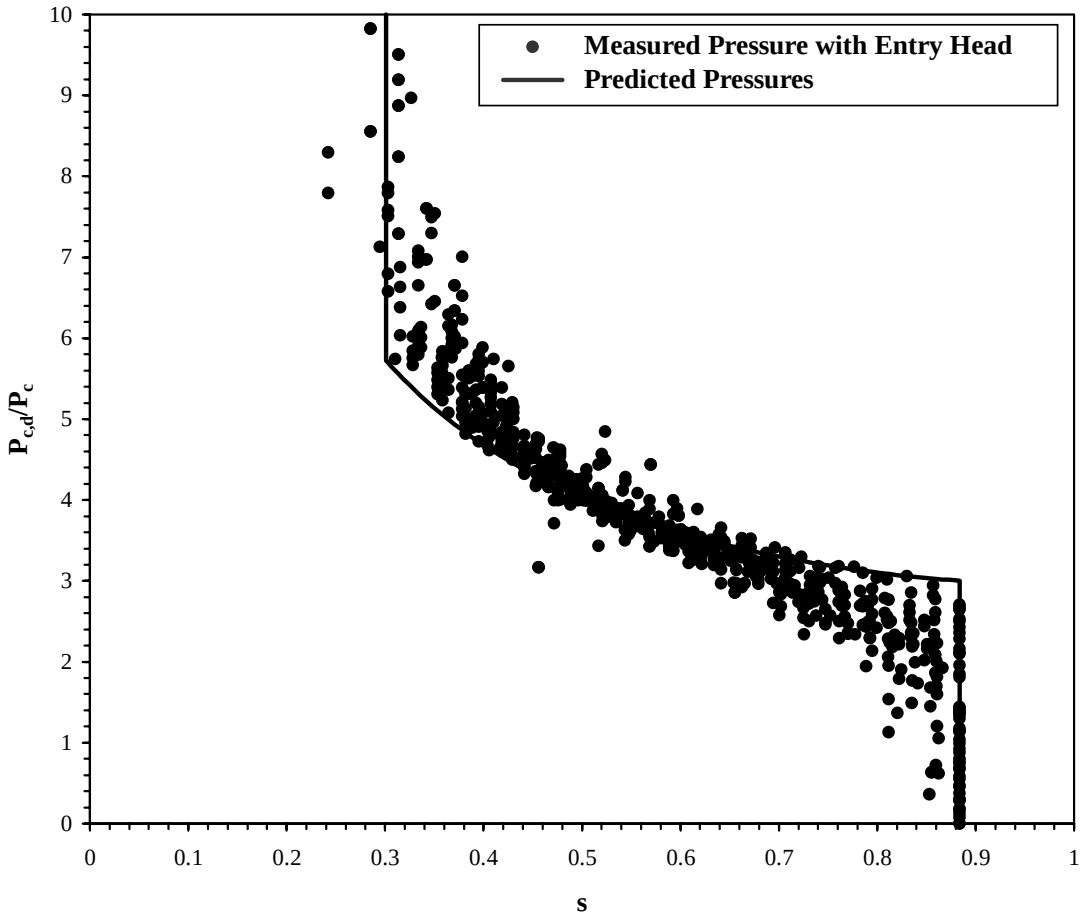

Figure 3. Comparison of UNSODA Field Drainage Data with Predicted Pressures

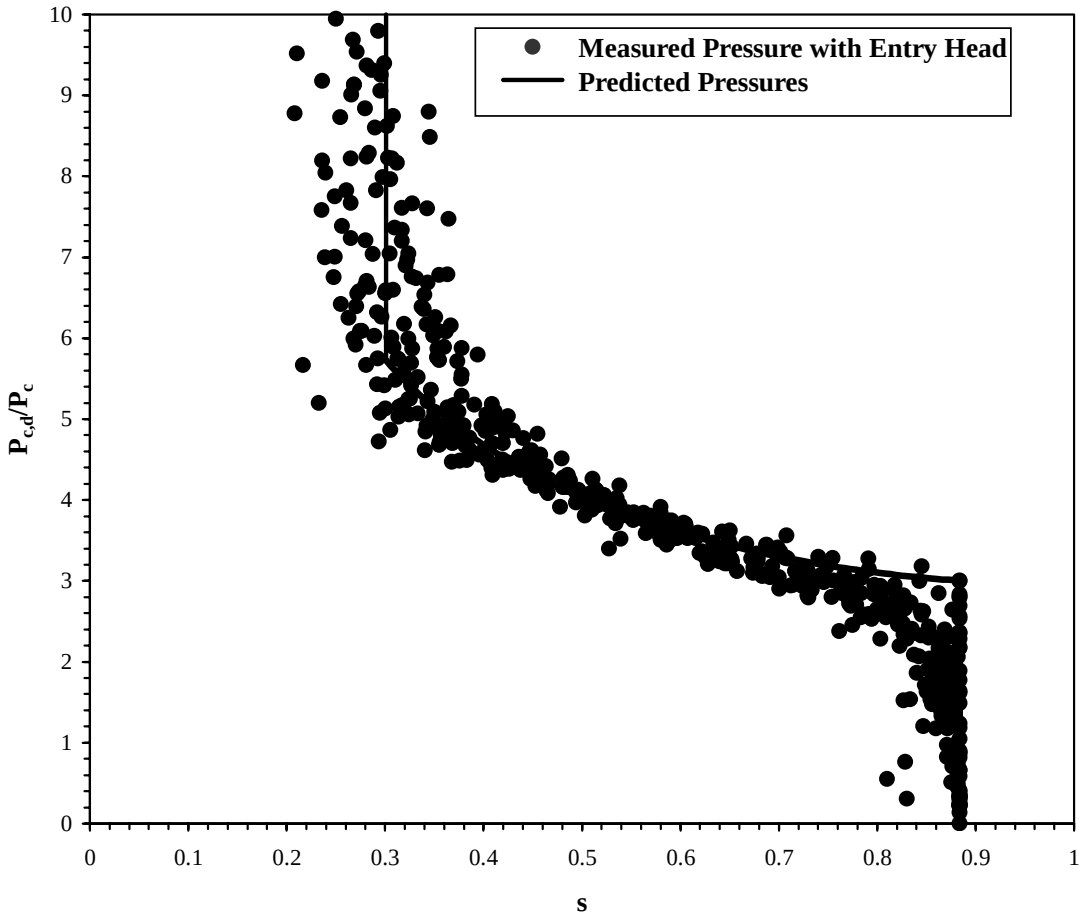

Figure 4. Comparison of UNSODA Laboratory Drainage Data with Predicted Pressures

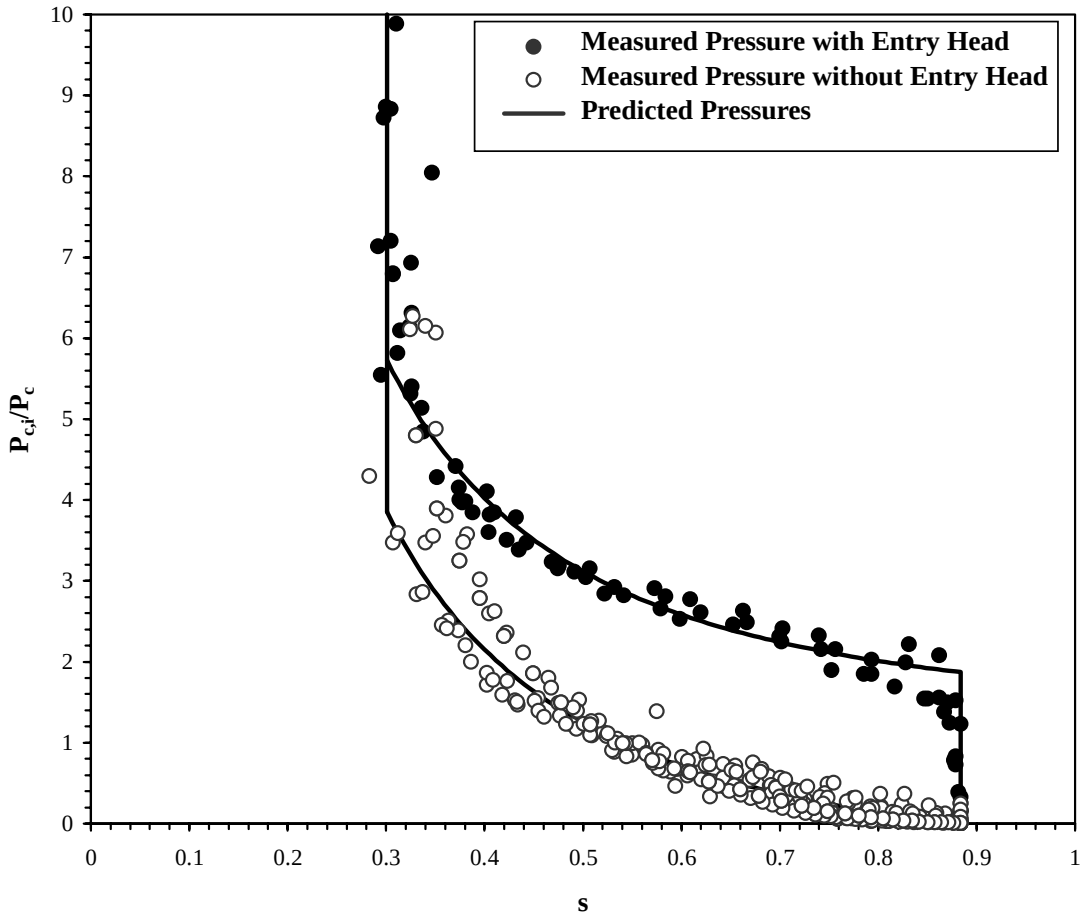

Figure 5. Comparison of UNSODA Laboratory Imbibition Data with Predicted Pressures

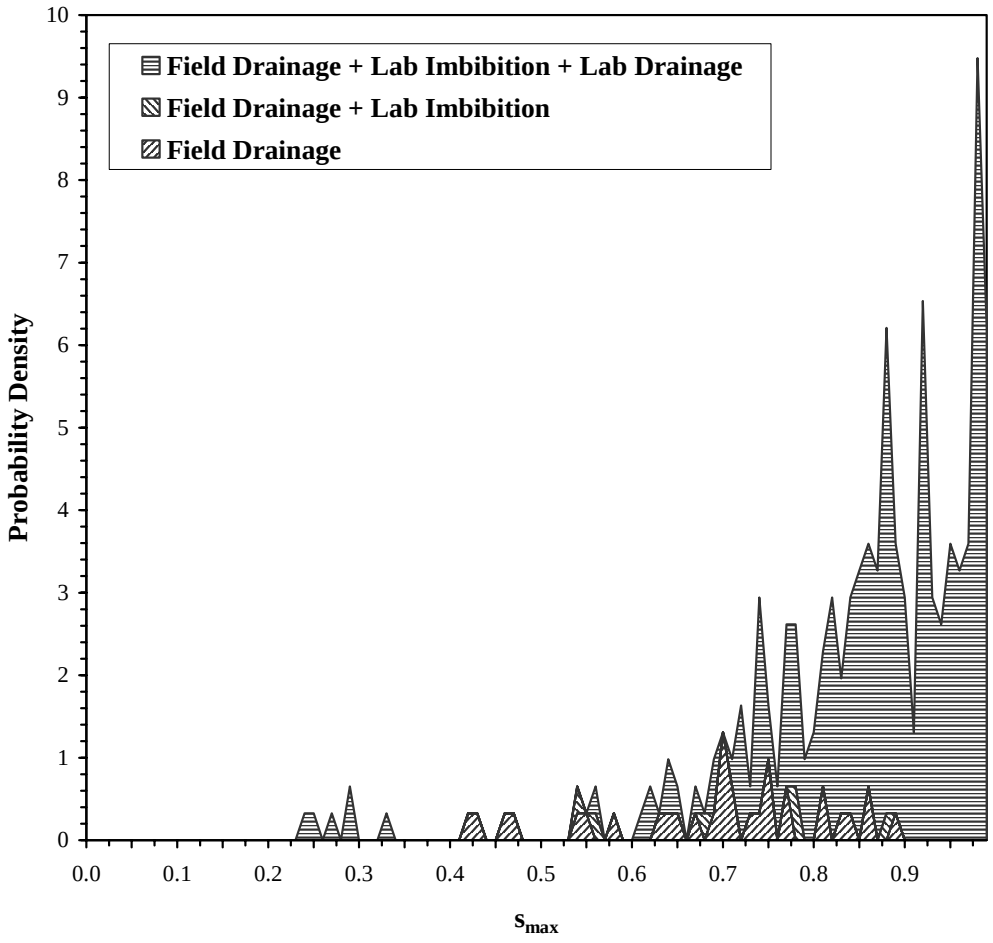

Figure 6. Distribution of Residual Nonwetting Saturations for the UNSODA Database, Using Porosities Based on Density Measurements (Based on 32 Field Drainage, 6 Lab Imbibition, and 268 Lab Drainage Data Sets)

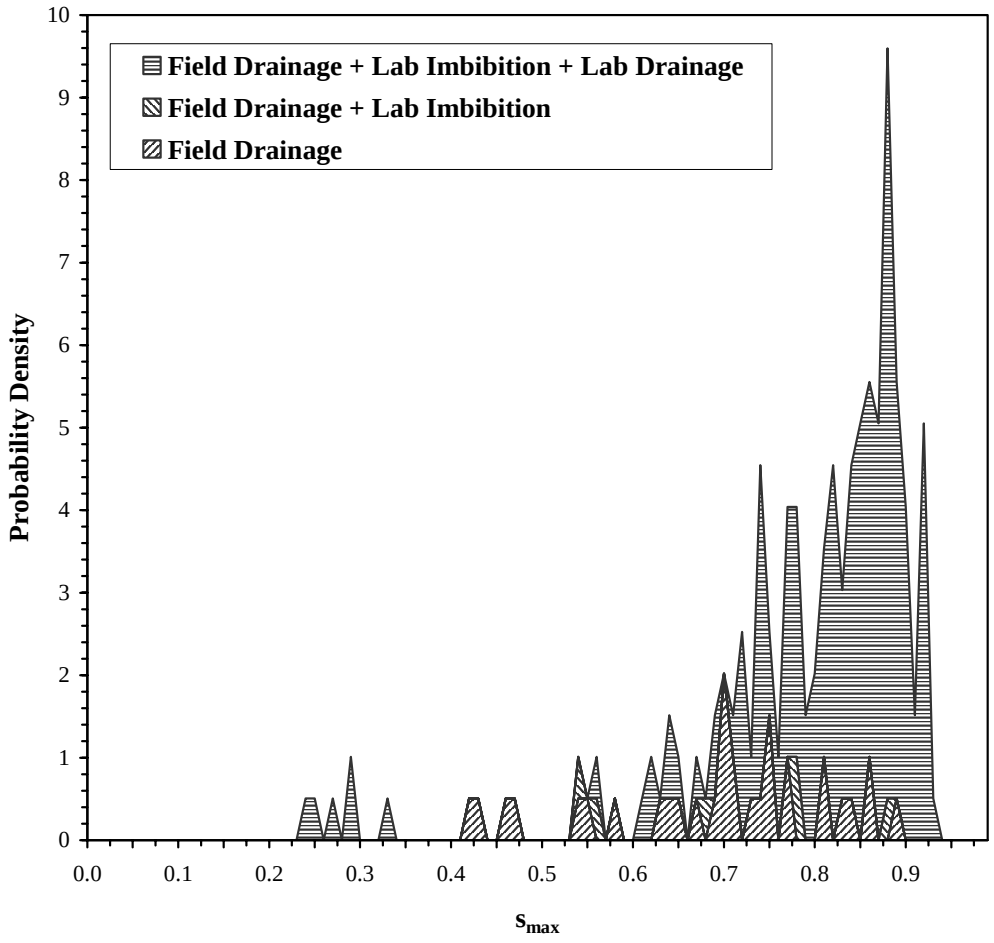

Figure 7. Distribution of Residual Nonwetting Saturations for the UNSODA Database, Using Porosities Based on Density Measurements, Measurements with Possible Presence of Residual Liquid Filtered Out (Based on 32 Field Drainage, 6 Lab Imbibition, and 160 Lab Drainage Data Sets)

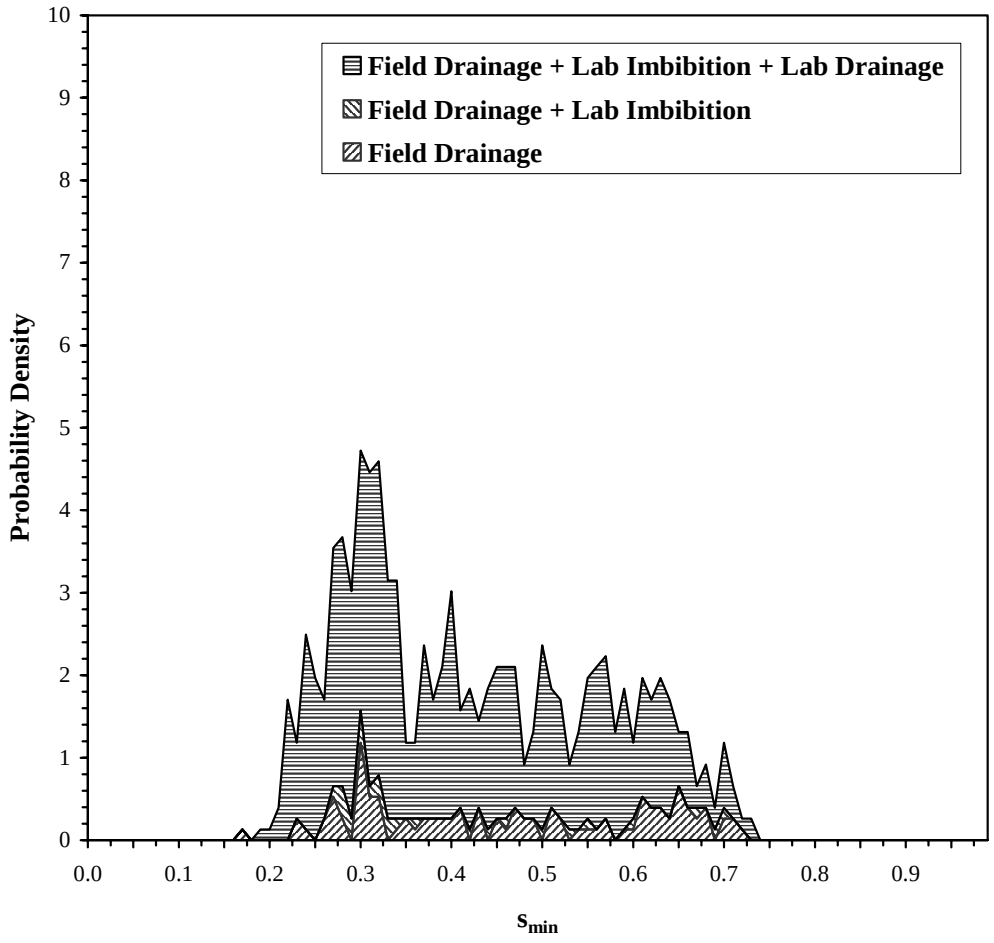

Figure 8. Distribution of Residual Wetting Saturations for the UNSODA Database, Assuming That $s_{max} = s_{rn}$ (Based on 99 Field Drainage, 26 Lab Imbibition, and 637 Lab Drainage Data Sets)

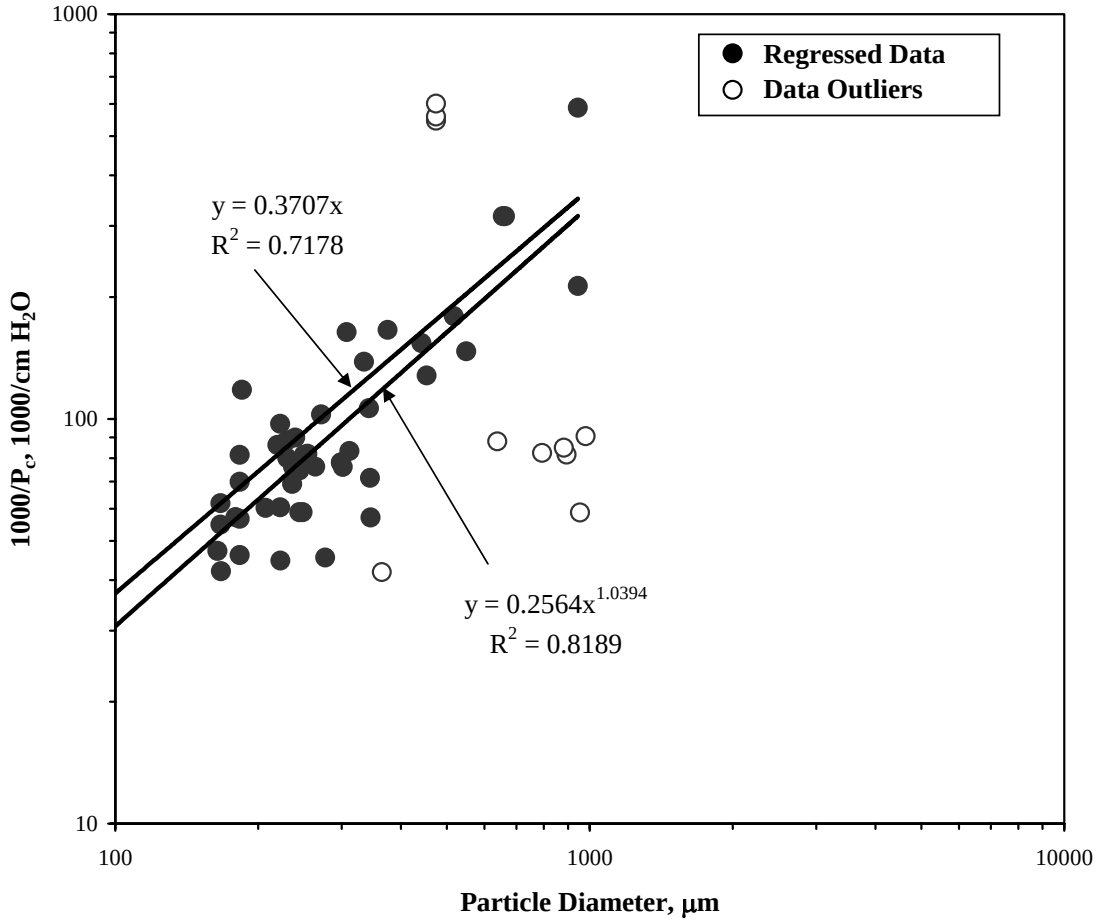

Figure 9. Correlation of Capillary Pore Pressures as a Function of Measured Particle Diameter, Pore Pressure Calculations Include Entry Heads